Published in final edited form as:
Neuroimage. 2012 February 1; 59(3): 2098–2109. doi:10.1016/j.neuroimage.2011.10.031.

MRI Patterns of Atrophy and Hypoperfusion Associations Across Brain Regions in Frontotemporal Dementia

Duygu Tosun[1,*], **Howard Rosen**[2,3], **Bruce L. Miller**[2,3], **Michael W. Weiner**[1,3,4], and **Norbert Schuff**[1,3,4]

[1]Center for Imaging Neurodegenerative Diseases, Veterans Affairs Medical Center, San Francisco, CA 94121, USA

[2]Memory and Aging Center, University of California San Francisco, San Francisco, CA 94143, USA

[3]Department of Neurology, University of California San Francisco, San Francisco, CA 94143, USA

[4]Department of Radiology, University of California San Francisco, San Francisco, CA 94143, USA

Abstract

Magnetic Resonance Imaging (MRI) provides various imaging modes to study the brain. We tested the benefits of a joint analysis of multimodality MRI data in combination with a large-scale analysis that involved simultaneously all image voxels using joint independent components analysis (jICA) and compared the outcome to results using conventional voxel-by-voxel unimodality tests. Specifically, we designed a jICA to decompose multimodality MRI data into independent components that explain joint variations between the image modalities as well as variations across brain regions. We tested the jICA design on structural and perfusion-weighted MRI data from 12 patients diagnosed with behavioral variant frontotemporal dementia (bvFTD) and 12 cognitively normal elderly individuals. While unimodality analyses showed widespread brain atrophy and hypoperfusion in the patients, jICA further revealed two significant joint components of variations between atrophy and hypoperfusion across brain regions. The 1st joint component revealed associated brain atrophy and hypoperfusion predominantly in the right brain hemisphere in behavioral variant frontotemporal dementia, and the 2nd joint component revealed greater atrophy relative to hypoperfusion affecting predominantly the left hemisphere in behavioral variant frontotemporal dementia. The patterns are consistent with the clinical symptoms of behavioral variant frontotemporal dementia that relate to asymmetric compromises of the left and right brain hemispheres. The joint components also revealed that that structural alterations can be associated with physiological alterations in spatially separated but potentially connected brain regions. Finally, jICA outperformed voxel-by-voxel unimodal tests significantly in terms of an effect size, separating the behavioral variant frontotemporal dementia patients from the controls. Taken together, the results demonstrate the benefit of multimodality MRI in conjunction with jICA for mapping neurodegeneration, which may lead ultimately to an improved

[*]Corresponding author: Duygu Tosun 4150 Clement St,San Francisco VA Medical Center Bldg 13, 114M San Francisco, CA 94121, USA duygu.tosun@ucsf.edu Office: (415) 221-4810 x4800 Fax: (415) 386-3954.

diagnosis of behavioral variant frontotemporal dementia and other forms of neurodegenerative diseases.

Keywords

Brain atrophy; Brain hypoperfusion; Dementia; Neurodegenerative diseases; Joint ICA; Multimodality MRI

Neurodegenerative diseases, such as Alzheimer's disease (AD), which impacts cognitive functions, and frontotemporal dementia (FTD), which impairs judgment and behavior, are a growing health problem globally as people live longer and the risk for these brain diseases increases dramatically with advancing age. Since a definite diagnosis of most forms of neurodegenerative diseases is currently only possible with autopsy, the development of biomarkers, which can reliably indicate presence of neurodegeneration at the earliest possible stage, is therefore an important public health goal. Structural magnetic resonance imaging (MRI) has widely been the method of choice to study neurodegenerative diseases, because macroscopically most neurodegenerative diseases are associated with progressive regional brain tissue loss that can be mapped with structural MRI [for a review see (Schuff and Zhu, 2007)]. In addition to brain tissue loss, neurodegenerative diseases typically exhibit also diminished brain function and reduced regional cerebral blood flow (rCBF), which can be detected non-invasively with perfusion-weighted MRI (Dai et al., 2009; Du et al., 2006; Johnson and Albert, 2000; Johnson et al., 2005; Lee et al., 2009; Tosun et al., 2010) as well as with radioactive tracer techniques, such as positron emission tomography (PET) or single photon emission computed tomography (SPECT) (Frisoni et al., 1995; Horn et al., 2009; Nagao et al., 2004; Varrone et al., 2002). Although various image modalities have provided a wealth of information about brain alterations associated with neurodegenerative diseases at the group level, the values of these measures for a clinical diagnosis at the individual level remain limited. A major challenge in this field is how to use and analyze data from multiple imaging modalities together in an integrated fashion that adds diagnostic value. Equally important to improving diagnosis is to gain deeper insight into the processes underlying neurodegeneration. For example, structural alterations in absence of functional deficits or vice versa could be extremely useful for staging the level of neurodegeneration and whether damage might be reversible, assuming appropriate medication will become available. Conventional univariate methods for image analysis are inefficient for assessments of structural and functional relationships, because each observation is evaluated separately. Moreover, conventional voxelwise statistical approaches, such as statistical parametric mapping (Worsley et al., 2004), lack the ability to detect hidden relationships across brain regions, a fundamental limitation considering the connectivity of the brain. Our main goal in this study was therefore to demonstrate the benefit of multivariate analysis of structural and physiological brain MRI data taken together for improvement in diagnosis of neurodegenerative diseases as well as gaining deeper insight into the biological substrates underpinning the disease. Therefore, we focus on the design of an integrated framework to exploit complementary information from structural and physiological brain MRI data toward an improvement in diagnosing neurodegenerative diseases.

As new tools for effective fusion of various MRI modalities, such as structural and perfusion-weighted MRI data, are emerging, more imaging studies aim at jointly analyzing data from multiple imaging modalities. For instance, several MRI studies examined the relationships between alteration in brain structure and physiology in aging and neurodegenerative diseases in region-of-interest or at voxel-by-voxel basis (Asllani et al., 2008; Chetelat et al., 2008; Eagger et al., 1992). Furthermore, to identify regions of concordance and discordance between structural and physiological brain changes in

neurodegenerative diseases without explicitly modeling the relationships, we developed functions to combine the statistics from different MRI modalities (Hayasaka et al., 2006). We recently applied this approach to study regional dissociations between brain atrophy and reduced rCBF in FTD, showing regionally varying reduction in rCBF despite widespread tissue atrophy (Shimizu et al., 2010). Moreover, to determine the added value of perfusion-weighted MRI beyond the value of structural MRI for the correct classification of AD, we performed cortical point-by-point tests based on logistic regressions to identify the regions where largely atrophy contributed to the classification and regions where reduced rCBF alone or in conjunction with atrophy made contributions (Tosun et al., 2010). However, the fundamental limitation that these studies have in common is the lack of simultaneous utilization of information from all brain regions (e.g., accounting for variations across voxels) and all imaging modalities (e.g., accounting for inter-modality correlations) to evaluate distributed relationships of structural and physiological alterations across the brain.

The purpose of the current study was to determine which brain regions with greater atrophy are associated with brain regions of reduced rCBF in patients with neurodegenerative diseases relative to controls. We also aimed to analyze all imaging voxels from both modalities simultaneously to capture not only variations across image modalities but also variations across brain regions. Specifically, we used multimodality joint independent component analysis (jICA) to reveal the pattern of regionally distributed associations between brain tissue loss (based on structural MRI) and rCBF (measured using arterial spin labeling (ASL) perfusion-weighted MRI) in patients with behavioral variant frontotemporal dementia (bvFTD), a sub-category of the frontotemporal lobar degeneration dementia complex, relative to cognitively normal elderly individuals. With jICA, patterns in one imaging modality can be evaluated while accounting simultaneously for variations in patterns seen in another imaging modality across the whole brain (Calhoun and Adali, 2009; Calhoun et al., 2006). Compared to voxelwise univariate and other multivariate analysis methods, the primary advantage of jICA is the ability to identify associations between image modalities across spatially separated brain regions without selecting regions a-priori. We choose behavioral variant frontotemporal dementia for this test, because previous imaging studies have implicated a signature pattern for each regional brain atrophy and rCBF deficits in patients with behavioral variant frontotemporal dementia (Cardenas et al., 2007; Chao et al., 2007; Du et al., 2006; Grimmer et al., 2004; Grossman et al., 2004; Ishii et al., 1998; Jeong et al., 2005; Nagao et al., 2004; Rosen et al., 2002; Varrone et al., 2002; Whitwell et al., 2005). These atrophy and rCBF patterns in behavioral variant frontotemporal dementia overlap partially but are also distinctly discordant (Shimizu et al., 2010) and therefore exhibit an attractive level of complexity to test if jICA can reveal large scale associations between alterations in structure and physiology across the brain in behavioral variant frontotemporal dementia. The specific objective of this study was twofold: (1) to determine the extent to which brain regions in behavioral variant frontotemporal dementia with greater atrophy than in controls are also associated with which brain regions with greater rCBF reduction using multimodality jICA and (2) to test if the brain regions identified by multimodality jICA provide a better discrimination between behavioral variant frontotemporal dementia patients and controls (i.e., effect size) than the regions identified by conventional unimodality analyses of structural and perfusion-weighted MRI data separately.

In this work, we will first present an integrated multimodality MR image-processing framework to preprocess the structural and perfusion-weighted MRI data for joint data analysis. Then, we will report the results from analysis of multimodality MRI data using multimodality jICA to identify significant relationships between regional alterations in brain tissue loss and reduced rCBF related to behavioral variant frontotemporal dementia. For comparison, we will also present unimodality analysis results evaluating the group

differences in brain tissue loss and reduced rCBF between behavioral variant frontotemporal dementia patients and controls followed by a quantitative comparison based on an effect size measure generalized to multimodality measures.

Methods

Subjects

Twelve behavioral variant frontotemporal dementia patients (mean age and standard deviation: 60.3 ± 7.6 years; 3 females / 9 males) and 12 controls (age: 60.9 ± 7.6yrs; 3 females / 9 males) were included in this cross-sectional multimodality MRI study. The behavioral variant frontotemporal dementia and control groups were pair-wise age and gender matched. A summary of the subject demographics and relevant clinical information are listed in Table 1. The subjects were recruited from the Memory and Aging Center of the University of California, San Francisco. All patients were diagnosed based upon information obtained from an extensive clinical history and physical examination. The structural MR images were used to rule out other major neuropathologies such as tumors, strokes, or inflammation but not to diagnose dementia. The subjects were included in the study if they were between 30–80 years old and without history of brain trauma, brain tumor, stroke, epilepsy, other types of dementia (Alzheimer's disease, vascular dementia, dementia with Lewy bodies), other neurodegenerative disorders (Huntington's disease, multiple system atrophy), alcoholism, psychiatric illness or other systemic diseases that affect brain function. The behavioral variant frontotemporal dementia patients were diagnosed according to the consensus criteria established by Neary et al., (Neary et al., 1998). In addition, the following selection criteria were included: (1) Clinical Dementia Rating (CDR) and Mini Mental State Examination (MMSE) completed within 90 days, (2) absence of comorbid motor neuron disease, (3) absence of logopenic progressive aphasia, and (4) absence of significant white matter hyperintensities (i.e. >3mm periventricular hyperintensities, or >10mm deep white matter lesions, or >10 lesions, as seen on FLAIR (fluid attenuated inversion recovery) images. Upper thresholds for WMSH were chosen based on the Scheltens scale to match the groups in terms of WMSH load.).

All subjects or their legal guardians gave written informed consent before participating in the study, which was approved by the Committees of Human Research at the University of California and the VA Medical Center at San Francisco.

Data Acquisition

All scans were performed on a 4 Tesla (Bruker /Siemens) MRI system with a birdcage transmit and 8 channel receive coil. The scans included T1-weighted (T1w) and T2-weighted (T2w) structural MRI data for measurements of brain atrophy and perfusion-weighted MRI for measurements of rCBF. T1w images were obtained with a 3D volumetric magnetization prepared rapid gradient echo (MPRAGE) sequence, TR/TE/TI = 2300/3/950 ms, timing; 7° flip angle; 1.0 × 1.0 × 1.0 mm^3 resolution; 157 continuous sagittal slices; acquisition time of 5 min. T2w images were acquired with a variable flip (VFL) angle turbo spin-echo sequence with TR/TE = 4000/30 ms and with the same resolution matrix and field of view of MPRAGE. In addition, FLAIR images with timing TR/TE/TI = 5000/355/1900 ms were acquired to facilitate the evaluation of white matter signal hyperintensities (WMSH) and the brain-extraction step in postprocessing.

Perfusion-weighted MR images were acquired using a continuous arterial spin labeling (cASL) sequence with single-shot echo-planar imaging (EPI), yielding sixteen 5 mm thick slices with 1.2 mm gaps and with an in-plane resolution of 3.75 × 3.75 mm^2. EPI timing was TR/TE = 5200/9 ms (Detre et al., 1992). For cASL, a 1.2 s long pulse with a magnetic field

strength of B1= 3.5×10^{-6} T was applied in the presence of a constant magnetic field gradient of 2 mT/m, followed by 1,590 ms post-labeling delay before the signal was mapped using EPI. Post-labeling delay of 1,590 ms was heuristically chosen to compensate for the prolonged arterial transit times in this age group (Detre and Alsop, 1999; Hunter et al., 1989). Note, since the acquisition of ALS is slice selective, the post-labeling delay increases linearly for each slice by about 45 ms. The labeling slice was fixed at 80 mm inferior to the central imaging slice. Forty control and 40 labeled scans were averaged to boost the signal-to-noise ratio resulting in a total scan time for cASL of about 7 minutes.

Structural MRI Processing

The following key processing steps were performed on each brain image volume for estimation of local tissue loss using deformation-based morphometry (DBM). First, an expectation maximization segmentation (EMS) algorithm including correction for intensity inhomogeneity (Van Leemput et al., 1999a, b) was applied to T1w with supplementary T2w image input, separating skull, scalp, extra-cranial tissue, cerebellum, and brain stem from the rest of brain image volume. Resulting brain image volume was voxel-wise classified into fractions of cerebral white matter (WM), cortical gray matter (GM), and sulcal cerebrospinal fluid (CSF). For subjects with WMSH, FLAIR images were also included as supplementary image input to aid the tissue classification. In presence of WMSH, tissue segmentation was augmented using WMSH information from FLAIR images. Out of 12 healthy controls, three required augmented tissue segmentation based on FLAIR due to presence of WMSH with total volumes between 1.04 cc and 1.76 cc. Similarly, out of 12 behavioral variant frontotemporal dementia patients, two required augmented tissue segmentation due to presence of WMSH with total volume between 6.83 cc and 6.28 cc. WMSH voxels were classified as WM tissue for the purpose of partial volume effect correction of rCBF images and to reduce bias in the vicinity of WMSH as explained in the following section.

Each individual skull-stripped and bias field corrected brain image volume was affine registered to a reference brain image to adjust for global differences in brain positioning and scale across individuals. For this study, an unbiased average brain image was used as the reference. The unbiased average brain was generated from 20 healthy elderly individual brains (i.e., age of 50 to 70) using an unbiased atlas formation technique based on large deformations mapping (Lorenzen et al., 2005). This set of 20 healthy elderly individuals did not include any controls studied in this work. A nonlinear inverse-consistent fluid-flow deformation (Lorenzen et al., 2005) spatially normalized affine registered individual brains to the reference brain. The Jacobian determinant of the deformation field (i.e., Jac-map), giving the fractional volume contraction or expansion at each voxel, was calculated to give a map of brain atrophy. A block diagram outlining the processing steps involved in DBM and a representative Jac-map for a healthy elderly control are provided in Figure 1. The Jac-maps were filtered using a Gaussian smoothing kernel, where the contribution of each neighboring Jac-map values to the center pixel was weighted by a Gaussian spatial kernel with a filter width of 6 mm FWHM in the reference brain image space. The size of the smoothing kernel matched the size of the effect we sought while accounting for residual errors in the nonlinear spatial normalization.

Integrated Multimodality Image Processing for Perfusion-Weighted MRI

The key processing steps for quantification of rCBF from cASL-MRI as outlined in the block diagram in Figure 2 and explained in detail elsewhere (Tosun et al., 2010) were as follows: For each subject, the labeled and control images were first rigidly (i.e., 6 degrees-of-freedom) realigned to the first image acquired in cASL sequence to correct for subject head positioning differences during scanning and then the mean labeled and mean control images were computed. The resulting mean control image was subtracted from the mean

labeled image, yielding raw perfusion-weighted image. This was followed by the intensity normalization of the raw perfusion-weighted image by the overall mean cASL image (i.e., average of mean labeled and mean control images) as approximation for arterial water density (Wen-Chau et al., 2009), and for elimination of spurious signal contributions of very high intensity from arterial vessels. The intensity normalization also reduced the intensity inhomogeneity in EPI. The perfusion-weighted signal was then intensity scaled to obtain a measure equivalent to rCBF, based on a single compartment model of cASL perfusion in which water exchange between capillaries and brain is instantaneous and homogeneous. To correct for variations in the cASL signal due to variable coverage of GM, WM and CSF at each voxel, the rCBF image was corrected for the tissue partial volume effects, which requires intra-subject inter-modality spatial alignment establishing a voxel-by-voxel anatomical correspondence between rCBF image space and structural MR image space where tissue densities (i.e., GM, WM, and CSF) were defined. To accomplish this, both mean control cASL image and rCBF image volumes were first mapped onto the T2w structural image space using a multi-resolution affine registration algorithm based on normalized mutual information. Since EPI-based perfusion images generally suffer from nonlinear geometric distortions due to variations in magnetic susceptibility whereas structural MR images suffer less from susceptibility distortions, the spatial alignment between the two modalities is a challenge. We used a fluid-flow warping based distortion correction algorithm, minimizing an image dissimilarity metric between the co-registered mean control cASL image and the T2w image (Lorenzen et al., 2005). The resulting nonlinear deformation vector field was applied to the affine registered rCBF image. Finally, the T2w image was rigidly aligned to the T1w image for domains with defined tissue densities and maps of brain atrophy. The T2w to T1w rigid alignment transformation was then applied to the nonlinear geometric distortion-corrected rCBF image. rCBF images in T1w image space were corrected for partial volume variations at each voxel based ($rCBF_{PVE}$) on the following two assumptions: (1) rCBF is a weighted linear combination of perfusion from GM and WM (i.e., $rCBF_{GM}$ and $rCBF_{WM}$, respectively), with the weighting coefficients expressing perfusion in terms of the corresponding tissue densities; and (2) the relationship between GM and WM perfusion is spatially constant (i.e, $CBF_{GM} = \kappa \times CBF_{WM}$ where κ=2.5 was used from literature values (Kanetaka et al., 2004)).

Representative map of $rCBF_{PVE}$ for a healthy elderly control is shown in Figure 2. Note, $rCBF_{PVE}$ is expressed in institutional rather than in absolute units of ml/100mg/min. Each subject's resulting $rCBF_{PVE}$ image was mapped onto the reference brain image space by applying the subject's structural spatial normalization based on the fluid-flow deformation [cf. Structural MRI Processing]. Each $rCBF_{PVE}$ map was intensity calibrated by setting its global median $rCBF_{PVE}$ to 1000, yielding rCBF*. The resultant rCBF* maps were filtered using a Gaussian smoothing kernel of 8 mm FWHM in the reference brain image space. A 3-to-4 ratio between Jac-map and rCBF* smoothing kernels was estimated as described in (Hagler Jr et al., 2006) to achieve comparable degrees of smoothing.

Unimodal Voxel-by-Voxel Group Analysis

The volumetric maps of Jac-map and rCBF* measures of each individual were analyzed separately using conventional univariate statistical parametric mapping. In this approach, differences in the maps between the behavioral variant frontotemporal dementia and control groups were examined voxel-by-voxel using a general linear model. Specifically, each brain map (i.e., Jac-map or rCBF*) was regressed separately at every brain tissue voxel against a categorical variable coding group membership as a predictor. To control for false positive findings given the large number of comparisons per brain map, we used the concept of a false discovery rate (FDR) at the level q=0.05 (Benjamini and Hochberg, 1995).

Unimodality statistical computations were carried out using the statistical package R (http://www.r-project.org/).

Multimodality Statistical Analysis

The objective of the multimodality statistical analysis is twofold: (1) We aim to analyze the imaging features from structural and perfusion-weighted MRI together to obtain complementary information from the structural and physiological relations not obtainable from separate unimodel group analysis of structural and physiological variations. Second, we aim to identify regional relationships between structural and physiological variations while simultaneously accounting for inter-voxel relationships across the brain, thus testing effectively for distributed relationships that voxel-by-voxel multivariate tests cannot provide. In this study, the imaging features are the Jac-map as an estimate of the brain atrophy and the rCBF* map as an estimate of the reduced brain physiology. In multimodality jICA, the Jac-map and rCBF* maps are treated as joint probability distributions of random observations. Under the assumption that the joint distributions can be decomposed into sets of spatially independent but joint sources of Jac-map and rCBF* features, multimodality jICA aims to estimate the joint mixing coefficients a_{ic} common to the Jac-map and rCBF* features. Formally, in jICA the signal of an image voxel v from an observation i using modality *k* (*i.e., k=Jac-map or rCBF**) is considered a linear combination of signals from *C* independent sources according to:

$$x_{iv}^{k}=\sum_{c=1}^{C}a_{ic}S_{cv}^{k},$$

where S_{cv}^{k} is the c^{th} independent source. Assuming mutual joint spatial independence of each modality, the relationship between multimodality MRI data and the sources can be expressed as a general model according to:

$$\left[X^{Jac-map}X^{rCBF*}\right]=A\cdot\left[S^{Jac-map}\mathrm{S}^{\mathrm{rCBF*}}\right]$$

or

$$\left[S^{Jac-map}\mathrm{S}^{rCBF*}\right]=W\cdot\left[X^{Jac-map}X^{rCBF*}\right]$$

where $W = A^{-1}$. Here, X^k is the k^{th} modality's observation data matrix of size N×V (i.e., number of subjects N times number of image voxels V), S^k is the k^{th} modality's source matrix of size C×V, and A is the unknown mixing matrix of size N×C with its inverse matrix W. Since the sources C and thus the columns of A are linearly independent, it follows that $(A^T \cdot A)$ is invertible and $W = (A^T \cdot A)^{-1} \cdot A^T$ is the transpose of A. We can further use the independence of the sources to write the joint probability density function of observation data as

$$p\left(x_1^{Jac-map},x_1^{rCBF*},\cdots,x_N^{Jac-map},x_N^{rCBF*}|W\right)=|\det W|\cdot p\left(x_1^{Jac-map},x_1^{rCBF*}\right)\cdots p\left(x_N^{Jac-map},x_N^{rCBF*}\right),$$

where $p(x_i^{Jac-map}, x_i^{rCBF*})$ is the joint probability density for subject *i*. A single optimal unmixing coefficient matrix W*, which fuses the information from multiple modalities, can be estimated by maximizing the following joint log-likelihood function:

$$W^* = \underset{W}{\operatorname{argmax}} \left\{ \log p\left(x_1^{Jac-map}, x_1^{rCBF*}, \cdots, x_N^{Jac-map}, x_N^{rCBF*} | W \right) \right\}.$$

In this study, Fusion ICA Toolbox (FIT), a freeware package (http://icatb.sourceforge.net/fusion), was used to perform data fusion and multimodality jICA to determine the shared variance between the Jac-map and rCBF* measures in relation to group differences (Calhoun et al., 2006). Specifically, we designed the jICA to decompose the joint distributions of Jac-map and rCBF* across all image voxels and subjects into independent components that explain joint variations between the two MRI modalities given variations across subjects as described above. jICA approach allows us to identify joint variations in atrophy and rCBF* measures across spatially separated brain regions.

Because of differences in image intensity ranges, Jac-map and rCBF* images were intensity normalized to have the same average sum-of-squares computed over all subjects and all brain image voxels for each modality separately. A single normalization factor is used per modality; thus, following normalization, the relative scaling within a given modality is preserved, but the units between modalities are the same in a least-squares sense. Intensity normalized Jac-map and rCBF* images were stacked into a large subject–voxel matrix (i.e., $[X^{Jac\text{-}map} X^{rCBF*}]$ matrix) as illustrated in Figure 3. A minimum description length criterion was used to estimate the number of joint sources (i.e., C) from the subject-voxel matrix (Li et al., 2007). The subject–voxel matrix was then decomposed linearly into a mixing matrix (i.e., A) and a source matrix (i.e., $[S^{Jac\text{-}map} S^{rCBF*}]$ matrix) using coefficient-constrained ICA (CC-ICA), which minimizes the mutual information of the output sources to achieve independence while simultaneously improving the estimation of group difference (Sui et al., 2009). In this decomposition, the Jac-map and rCBF* within each joint source (i.e., each row of the source matrix) had the same shared contribution to the subjects, captured by the loading parameter within each column of the mixing matrix. In other words, each joint source provides the brain regions where Jac-map and rCBF* were associated by the same inter-subject covariation.

For each joint source, a two-sample t-test was performed on the loading parameters from the corresponding column of the mixing matrix to test the significance of the joint source in differentiating the behavioral variant frontotemporal dementia patients from the healthy elderly controls. For spatial visualization of the joint sources, each row of the source matrix was scaled to unit standard deviation, yielding z-score maps. Entries of each row were mapped back to the voxel coordinates to reconstruct the spatial localization of the joint sources of Jac-map and rCBF* in the reference brain image space.

A Multimodality Effect Size Measure

To evaluate the power of differences between the groups with information from both imaging modalities, we computed an effect size metric generalized to multimodality data, based on the multivariate analysis of variance (MANOVA) Wilks' lambda. For each significant joint component identified by jICA, mean Jac-map and mean rCBF* values were computed for each subject over joint source voxels with z-score values greater than or equal to 2.5 (99.4% cumulative probability). Subjects' mean Jac-map and mean rCBF* values formed the vectors of observations. In a one-way MANOVA with the vectors of observations as the dependent variable and the diagnosis as the categorical variable, Wilks' lambda, L, was estimated as the within groups generalized variance relative to the total generalized variance. A generalized Fisher's correlation ratio, $\eta^2_\Lambda = 1 - \Lambda$, was calculated giving the proportion of the total generalized variance, which is accounted for by the

population group membership (Steyn and Ellis, 2009). While a η^2_Λ of value 0.02 was considered as a small effect size and a η^2_Λ of value 0.13 was considered as a medium effect size, η^2_Λ greater than 0.26 was considered as a large effect size between behavioral variant frontotemporal dementia patients and controls (Steyn and Ellis, 2009).

Similarly for multimodality effect size of brain tissue loss and reduced rCBF* identified by separate unimodality group analysis, we computed the subject mean Jac-map and mean rCBF* values over the voxels where unimodality group analysis gave a corrected p value less than or equal to 0.005. Using the resulting subject vectors of observations, the generalized Fisher's correlation ratio was computed as explained above.

Results

Unimodal voxel-by-voxel Group Differences

Figures 4a and 4b depict the regional distributions of atrophy and reduced rCBF* in behavioral variant frontotemporal dementia patients compared to controls, respectively, using conventional univariate parametric statistical mapping. Consistent with several earlier MRI studies (Cardenas et al., 2007; Chao et al., 2007; Du et al., 2006; Grimmer et al., 2004; Grossman et al., 2004; Ishii et al., 1998; Jeong et al., 2005; Nagao et al., 2004; Rosen et al., 2002; Varrone et al., 2002; Whitwell et al., 2005), behavioral variant frontotemporal dementia patients showed greater ventricular enlargement and widespread brain tissue loss compared to controls predominantly in the frontal, temporal, and parietal brain regions as listed in Table 2. Significantly reduced rCBF* in behavioral variant frontotemporal dementia patients compared to controls occurred prominently in the bilateral frontal and temporal cortices as listed in Table II as well as in the thalamic nuclei, putamen, caudate, and hippocampal subcortical regions, consistent with findings from previous studies including PET and SPECT studies (Cardenas et al., 2007; Du et al., 2006; Gorno-Tempini et al., 2004; Grimmer et al., 2004; Ishii et al., 1998; Kril and Halliday, 2004; Mummery et al., 2000; Rabinovici et al., 2008; Rosen et al., 2002; Varma et al., 2002)

Multimodality Joint Independent Components Analysis

Among the estimated twenty-three joint independent components, the jICA analysis identified two joint components, each depicting associations between brain atrophy (i.e., Jacmap) and reduced rCBF* that were significantly different between behavioral variant frontotemporal dementia and controls.

The mixing coefficients of the 1^{st} joint component were 0.644 ± 0.047 for controls and 0.389 ± 0.067 for behavioral variant frontotemporal dementia patients with $t_{22}=-3.834$ and $p=0.0009$. Fig. 5 displays the spatial extent of the 1^{st} joint component's features at $z=2.5$ (99.4% cumulative probability) threshold, overlaid onto the reference brain image. The marginal Jac-map and rCBF* histograms computed by ranking voxels surviving the $z=2.5$ threshold are shown in Fig. 5c. In the 1st joint component, brain regions with greater white matter and gray matter atrophy in behavioral variant frontotemporal dementia patients compared to controls included areas prominently in the right hemisphere with greater caudate nucleus atrophy and ventricular enlargement bilaterally. Greater tissue loss in this component was linked to associated reduction in rCBF* (e.g., variations in each measure occur together) in behavioral variant frontotemporal dementia patients relative to controls prominently in the bilateral middle frontal, anterior cingulate, caudate nucleus, and thalamic nuclei, and right frontal cortical regions and insular regions as listed in Table 2.

The mixing coefficients of the 2^{nd} joint component were 0.461 ± 0.045 for controls and 0.290 ± 0.064 for behavioral variant frontotemporal dementia patients with $t_{22}=-2.65$ and $p=0.01$. Fig. 6 displays the spatial extend of 2^{nd} joint component's features at $z=2.5$

threshold overlaid onto reference brain image and the marginal Jac-map and rCBF* histograms are shown in Fig. 6c. The 2nd component reflects the relationship between greater atrophy and reduced rCBF* prominently in the left hemisphere brain regions as listed in Table 2.

Multimodality Effect Size

Multimodality effect sizes to separate behavioral variant frontotemporal dementia patients from controls based on regional brain atrophy and reduced rCBF* measures identified by the 1^{st} and 2^{nd} joint components are listed in Table 3. MANOVA Wilks' lambda and generalized Fisher's correlation ratio as a measure of multimodality effect size are reported. Also shown in Table 3 is the effect size based on conventional unimodal statistical parametric mapping for comparison. The statistical distribution of each multimodality effect size measure was numerically estimated by 100-fold bootstrapping. While brain atrophy and rCBF* differences jointly observed by the 1^{st} and 2^{nd} multimodality jICA components yielded large effect sizes, the corresponding effect sizes observed for unimodal tests were much smaller. Two-sample t-test revealed that all pair-wise multimodality effect size differences were statistically significant (separate unimodal tests versus 1^{st} joint component: $t=-15.06$, $df = 197.12$, $p<10^{-15}$; separate unimodal tests versus 2^{nd} joint component: $t=-8.95$, $df = 195.38$, $p<10^{-15}$; 1^{st} joint component versus 2^{nd} joint component: $t=4.89$, $df=191.69$, $p<10^{-5}$).

4. Discussion

This study generated two major findings: First, using multimodality jICA we found two behavioral variant frontotemporal dementia-related joint components of structural and physiological alterations in the brain. The 1^{st} joint component revealed an association between brain tissue loss and reduced rCBF* predominantly in the right brain hemisphere in behavioral variant frontotemporal dementia, and the 2^{nd} joint component revealed greater atrophy relative to reduced rCBF* affecting predominantly the left hemisphere in behavioral variant frontotemporal dementia. The difference in the mixing coefficients between behavioral variant frontotemporal dementia and controls, reflecting an atrophy/rCBF association, was largest for the 1^{st} joint component. The result is consistent with the fact that behavioral variant frontotemporal dementia tends to affect the right hemisphere more severely than the left, leading to problems with socioemotional behavior early in the disease course (Rosen et al., 2005). Moreover, the joint components revealed that structural alterations can be associated with physiological alterations in spatially separated but potentially connected regions. The second, and perhaps most important finding is that identification of joint components across structural and perfusion-weighted MRI resulted in a significant increase in effect size separating behavioral variant frontotemporal dementia patients from controls compared to the effect size derived using a conventional univariate analysis separately for each modality. Taken together, the results demonstrate the benefit of using multimodality MRI in conjunction with jICA for mapping neurodegeneration. This may lead ultimately to an improved diagnosis of behavioral variant frontotemporal dementia and other forms of dementia.

Our first finding with multimodality jICA extends our earlier MRI findings of partially dissociated structural and physiological alteration in behavioral variant frontotemporal dementia based on simply combining the statistics from structural and perfusion MRI (Shimizu et al., 2010). The observed dissociations involved substantial atrophy in absence of rCBF* reduction in some brain regions in behavioral variant frontotemporal dementia while other brain regions showed concordant levels of atrophy and rCBF* reductions. However, the previous approach was limited to observations of local relationships between structural and physiological alterations while relationships across brain regions were not accessible. Multimodality jICA can eloquently overcome this restriction, yielding a wealth of new

information of structural and physiological relationships not only at a local level but across distal brain regions as well. Especially the evaluation of all brain regions simultaneous provides a powerful tool for new discoveries, as the findings from the 1st and 2nd jICA components demonstrate.

The findings of associated structural and physiological brain alterations with multimodality jICA are worth more discussion and clinical interpretation. The joint component with the strongest behavioral variant frontotemporal dementia related alterations relative to the control group (i.e., 1st joint component) identified significant brain atrophy in the right frontal and limbic lobes, insular, and caudate regions as well as marked ventricular enlargement in the patients. These brain structure changes were linked to a concurrent reduction in rCBF* of the same anatomical regions in the right cortical hemisphere and subcortical regions including the thalamus and caudate. The findings suggest that certain effects of neurodegenerative disease serve as a substrate both for morphological and physiological changes in behavioral variant frontotemporal dementia. The findings in the ventromedial frontal, dorsolateral prefrontal, insula, and anterior cingulate brain regions can be related to the apathy and stereotypic behaviors, which are the most common initial symptoms among patients with behavioral variant frontotemporal dementia (Rosen et al., 2005; Shinagawa et al., 2006).

jICA analysis also found a second joint component whose expression differed with diagnosis, providing complementary information to the first component. Specifically, the 2nd joint component showed behavioral variant frontotemporal dementia related alterations relative to alterations in the control group that involved greater brain atrophy in the left hemisphere. The affected regions included the frontal, temporal, limbic, and parietal lobes, motor cortex, and hippocampus in addition to ventricular enlargement prominently in the posterior horns in behavioral variant frontotemporal dementia compared to controls. These regional brain tissue losses were linked to reduced rCBF* in similar anatomical regions again prominently in the left hemisphere. The finding of two distinct joint components of linked structural and physiological alterations implies that the pathology in behavioral variant frontotemporal dementia underlying these changes spreads heterogeneously across the right and left hemispheres. While the majority of frontal and limbic lobe regions are affected early in behavioral variant frontotemporal dementia, the temporal and parietal lobe regions are affected later in the disease process (Kril and Halliday, 2004). Accordingly, one can hypothesize that while the 1st joint component identified the brain regions affected during the early disease stage, the 2nd joint component identified the atrophy and reduced rCBF* occurring in the middle and later stages. The group of behavioral variant frontotemporal dementia patients studied in this work is very heterogeneous in terms of the duration of symptoms (i.e., standard deviation of 4.7 years). The outcome measures (i.e., local brain atrophy and perfusion) in behavioral variant frontotemporal dementia group may be affected by the duration of symptoms; hence, treating this set of subjects as a single group may not be adequate. Future longitudinal studies are warranted to elucidate a possible link between multimodality jICA components and temporal ordering of the behavioral variant frontotemporal dementia-related neuropathology. It is also possible that the components could represent different anatomical variants of behavioral variant frontotemporal dementia. The interpretation of these components would be greatly improved by a future investigation on whether the two components correlate with clinical/behavioral deficits in these patients.

Involvement of parietal, pre- and postcentral, cerebellar, and occipital region suggests that the patients in this study cohort were more demented than they appeared based on their widely used CDR scores, which may underrate disease severity in behavioral variant frontotemporal dementia. This phenomeon was also reported in other studies (Knopman et al., 2008; Mioshi et al., 2010). The length of symptoms might be a better proxy for disease

severity. Given the long disease history of the behavioral variant frontotemporal dementia patients in this study, these patients most likely fell into the severe to very severe disease categories. Based on clinicopathological staging of FTD severity (Kril and Halliday, 2004), we therefore find the involvement of these regions not surprising, especially since they show much weaker effects than the more prominently affected regions, including the frontal, temporal, and limbic lobes. Behavioral variant frontotemporal dementia is heterogeneous in terms of underlying pathology; peri-rolandic and parietal involvement might suggest underlying corticobasal degeneration (CBD), a common cause of behavioral variant frontotemporal dementia. Cerebellum might be seen in progressive supranuclear palsy (PSP), which can present clinically as behavioral variant frontotemporal dementia. Occipital findings were surprising to us too. Although our clinical accuracy is around 93% compare to autopsy, it is possible that some cases have additional Alzheimer's disease pathology. bvFTD shares many clinical and radiological features with CBD and PSP (Kitagaki et al., 2000; Cordato et al., 2005). Without a histopathological exam, these common features could make both clinical and radiological diagnosis difficult to distinguish these neurodegenerative disorders (Kertesz et al., 2000; Mathuranath et al., 2000).

Another interesting observation is the right- and left-sided asymmetry in 1st and 2nd joint components, respectively. Patients with behavioral variant frontotemporal dementia often present impaired behavioral symptoms that are consistent with an asymmetric left or right-sided structural and physiological abnormalities. For example, it has been shown that patients with primarily right versus left behavioral variant frontotemporal dementia have unique neuropsychological characteristics (Boone et al., 1999). More studies are warranted to further investigate the link between asymmetry in imaging findings and neuropsychological characteristics.

Our findings of morphometric and physiological alterations in behavioral variant frontotemporal dementia based on conventional voxel-by-voxel unimodal analysis yields two interesting aspects. First, the unimodal analysis of Jac-map and rCBF* maps, showing frontal and anterior temporal predominant but widespread structural atrophy and rCBF* reduction in the behavioral variant frontotemporal dementia patients compared to the controls, is consistent with findings from previous studies including PET and SPECT studies (Cardenas et al., 2007; Du et al., 2006; Gorno-Tempini et al., 2004; Grimmer et al., 2004; Ishii et al., 1998; Kril and Halliday, 2004; Mummery et al., 2000; Rabinovici et al., 2008; Rosen et al., 2002; Varma et al., 2002), implying that our patient group is a representative sample of behavioral variant frontotemporal dementia. Second, although the conventional analysis approach yielded large clusters of brain alterations in behavioral variant frontotemporal dementia, it largely missed the inherent hemispheric asymmetry of deficits in behavioral variant frontotemporal dementia that jICA revealed. The shortfall in sensitivity with the conventional method is not surprising given that each region is tested separately and associations across regions cannot be inferred. Although our anatomical localizations of regional atrophy and decreased perfusion findings in behavioral variant frontotemporal dementia compared to healthy elderly controls using multimodality jICA are in conformity with findings reported in the literature, the joint components were identified by simultaneously evaluating the imaging measures from both imaging modalities as well as across all brain regions thereby taking intrinsic relationships between these imaging measures into consideration. Therefore our multimodality jICA findings provide deeper insight into the biology of the disease than the methods, which evaluate the modalities as well as each brain region separately.

The second and perhaps most important finding of the study is the gain in effect size using jICA. The results imply that joint analysis of multimodality MRI data provides unique morphological and physiological signatures with significantly larger effect sizes than a

conventional approach. For diagnostic purposes, an important question is to what extent imaging modalities other than structural MRI provide “added value”. Although the current study does not explicitly address this question, comparisons based on effect sizes to separate behavioral variant frontotemporal dementia patients from controls suggest that a joint analysis of structural and perfusion-weighted MRI using multimodality jICA is more powerful than other analytical methods, especially those that evaluate structural and perfusion-weighted MRI separately. The improvement with multimodality jICA in identifying behavioral variant frontotemporal dementia likely derives from the ability to detect joint structural and physiological variations in behavioral variant frontotemporal dementia across brain regions that are involved in the neuronal network impacted by the disease (Schroeter et al., 2009). Whether this feature of multimodality jICA improves differential diagnosis between behavioral variant frontotemporal dementia and other forms of dementia causing neurodegenerative diseases, such as AD, which impacts other neuronal networks, warrants further investigation. The fact that it is not necessary to predefine these regions a-priori for multimodality jICA is another advantage of this approach. Identifying the multimodality imaging biomarkers (e.g., patterns of anatomical and physiological abnormalities) with predictive value for the development and progression of the disease could enhance the differential diagnosis accuracy for neurodegenerative diseases.

To our knowledge, our study is the first using jICA for the joint analysis of structural and perfusion-weighted MRI data. Furthermore, we incorporated jICA into a framework of integrated multimodality MR image-processing. The present study demonstrates that more information for the characterization and classification of behavioral variant frontotemporal dementia can be gained with this new approach. The application of jICA of multimodality imaging data is not limited to classification problems but can also be employed in principle to regression issues, such as identifying the correlates between structural and physiological changes and clinical and cognitive measures such as socioemotional or cognitive abilities.

The present study has several limitations. First, behavioral variant frontotemporal dementia was identified by clinical diagnosis but was not autopsy-confirmed. Therefore, to the extent that the diagnosis was inaccurate, the structural and physiological features from multimodality jICA may reflect other pathologies than behavioral variant frontotemporal dementia. We have autopsy confirmed pathology for three of the behavioral variant frontotemporal dementia patients. An additional five of the patients, plus another one who also had behavioral variant frontotemporal dementia confirmed by autopsy, went through PiB-PET imaging and had amyloid-negative results, implying no Alzheimer's disease pathology. In addition, two of these amyloid-negative behavioral variant frontotemporal dementia patients had lumbar Tau/Aβ ratio of 0.2 and 0.36, which do not fall into the Alzheimer's disease range. Although we cannot warrant that no Alzheimer's pathology was involved, 8 out of 12 behavioral variant frontotemporal dementia patients had no signs of Alzheimer's disease pathology and therefore our observations cannot be explained by presence of Alzheimer's disease alone. Second, the behavioral variant frontotemporal dementia patient sample is relatively small owing to difficulties in recruiting these patients, who often have behavioral and emotional disturbances, and compliance issues with participating in MRI. Therefore, generalization of our findings is limited. Further studies, including more subjects as well as behavioral variant frontotemporal dementia patients with a greater range of cognitive deficits, are warranted to validate the findings. There are additional study limitations related to the jICA technique. The current framework assumes that both image voxels and measures from each modality (i.e., Jac-map and rCBF*) are independent and identically distributed. A priori spatial correlation information and flexible distribution for each imaging measure could be incorporated to multimodality jICA to further improve the detection of multimodality imaging signatures. The inherent spatial smoothness of the data due to the point spread function of MRI, as well as the Gaussian

kernel-based smoothing used for image processing introduce spurious dependencies among the samples, thereby violating to some extent the rules of component selection that are based on the assumption of independent and identically distributed samples. Thus, both smoothing factors may have caused an overestimation of the number of independent components and therefore the results should be interpreted with caution. Another study limitation is that rCBF* measurements with cASL-MRI are susceptible to age-related variations in physiological conditions, such as arterial transit delays, altered T1 relaxation, and bolus dispersion, which are complicated to account for. In particular, age associated changes in relaxation times of blood water (Cho et al., 1997) and prolonged arterial transit time has been observed in behavioral variant frontotemporal dementia patients (Hunter et al., 1989). Therefore, we cannot rule out that some variations in rCBF* are simply measurement artifacts that are unrelated to differences in brain function between behavioral variant frontotemporal dementia patients and controls. In addition, nine out of 12 behavioral variant frontotemporal dementia patients were receiving various drugs known to impact the cardiovascular system. Due to the small sample size of this study and limited statistical power, we couldn't control for effects of medication on arterial blood flow. Furthermore, in integrated multimodality MR image processing, the accuracy of the intra-subject inter-modality co-registration is limited since cASL-MRI is more prone to geometric distortion and imaging artifacts compared to structural MRI. The partial volume correction and anatomical localization in rCBF* measure is also limited by the differences in point spread function of structural and perfusion-weighted MRIs. In addition, structural spatial normalization accuracy and consequently accurate partial-volume correction might be compromised in behavioral variant frontotemporal dementia patients as a result of averaging across dissimilar structures. Thus, changes in brain morphology may have biased rCBF* measurements. Taken together, errors in image registration and localization may result in diminished power to detect intrinsic relationships between structural and physiological alterations in behavioral variant frontotemporal dementia at a local level. Lastly, this study was cross-sectional and cannot conclusively establish causality between structural and physiological alterations. Longitudinal studies will be necessary to further understand the synergistic effects of anatomical and physiological changes in behavioral variant frontotemporal dementia patients.

Despite these limitations, our results specifically demonstrate the benefit of jICA of multimodality MRI and to enhance the description of pathophysiological changes in neurodegenerative disease, which may ultimately lead to improved diagnostic methods. Beyond the study of neurodegenerative diseases, integrated multimodality image analysis methods could be useful in the evaluation of other brain disorders as well as pathology in other body systems.

Acknowledgments

This work was supported by the National Institutes of Health grant P41 RR23953 and P01 AG019724, and the Department of Defense grant W81XWH-05-2-0094. This work has also been made possible by use of research facilities at the Veteran Affairs Medical Center in San Francisco.

References

Asllani I, Habeck C, Scarmeas N, Borogovac A, Brown TR, Stern Y. Multivariate and univariate analysis of continuous arterial spin labeling perfusion MRI in Alzheimer's disease. J Cereb Blood Flow Metab. 2008; 28:725–736. [PubMed: 17960142]

Benjamini Y, Hochberg Y. Controlling the False Discovery Rate: A Practical and Powerful Approach to Multiple Testing. Journal of the Royal Statistical Society. Series B (Methodological). 1995; 57:289–300.

Boone KB, Miller BL, Lee A, Berman N, Sherman D, Stuss D. Neuropsychological patterns in right versus left frontotemporal dementia. Journal of the International Neuropsychological Society. 1999; 5:616–622. [PubMed: 10645704]

Calhoun VD, Adali T. Feature-Based Fusion of Medical Imaging Data. Information Technology in Biomedicine, IEEE Transactions on 13. 2009:711–720.

Calhoun VD, Adali T, Giuliani NR, Pekar JJ, Kiehl KA, Pearlson GD. Method for multimodal analysis of independent source differences in schizophrenia: Combining gray matter structural and auditory oddball functional data. Human Brain Mapping. 2006; 27:47–62. [PubMed: 16108017]

Cardenas VA, Boxer AL, Chao LL, Gorno-Tempini ML, Miller BL, Weiner MW, Studholme C. Deformation-Based Morphometry Reveals Brain Atrophy in Frontotemporal Dementia. Arch Neurol. 2007; 64:873–877. [PubMed: 17562936]

Chao LL, Schuff N, Clevenger EM, Mueller SG, Rosen HJ, Gorno-Tempini ML, Kramer JH, Miller BL, Weiner MW. Patterns of White Matter Atrophy in Frontotemporal Lobar Degeneration. Arch Neurol. 2007; 64:1619–1624. [PubMed: 17998444]

Chetelat G, Desgranges B, Landeau B, Mezenge F, Poline JB, de la Sayette V, Viader F, Eustache F, Baron J-C. Direct voxel-based comparison between grey matter hypometabolism and atrophy in Alzheimer's disease. Brain. 2008; 131:60–71. [PubMed: 18063588]

Cho S, Jones D, Reddick WE, Ogg RJ, Steen RG. Establishing norms for age-related changes in proton T1 of human brain tissue in vivo. Magnetic Resonance Imaging. 1997; 15:1133–1143. [PubMed: 9408134]

Dai W, Lopez OL, Carmichael OT, Becker JT, Kuller LH, Gach HM. Mild Cognitive Impairment and Alzheimer Disease: Patterns of Altered Cerebral Blood Flow at MR Imaging. Radiology. 2009; 250:856–866. [PubMed: 19164119]

Detre JA, Alsop DC. Perfusion magnetic resonance imaging with continuous arterial spin labeling: methods and clinical applications in the central nervous system. European Journal of Radiology. 1999; 30:115–124. [PubMed: 10401592]

Detre JA, Leigh JS, Williams DS, Koretsky AP. Perfusion imaging. Magnetic Resonance in Medicine. 1992; 23:37–45. [PubMed: 1734182]

Du AT, Jahng GH, Hayasaka S, Kramer JH, Rosen HJ, Gorno-Tempini ML, Rankin KP, Miller BL, Weiner MW, Schuff N. Hypoperfusion in frontotemporal dementia and Alzheimer disease by arterial spin labeling MRI. Neurology. 2006; 67:1215–1220. [PubMed: 17030755]

Eagger S, Syed GM, Burns A, Barrett JJ, Levy R. Morphologic (CT) and functional (rCBF-SPECT) correlates in Alzheimer's disease. Nucl Med Commun. 1992; 13:644–647. [PubMed: 1448236]

Frisoni GB, Pizzolato G, Geroldi C, Rossato A, Bianchetti A, Trabucchi M. Dementia of the frontal type: neuropsychological and [99Tc]-HM-PAO SPET features. J Geriatr Psychiatry Neurol. 1995; 8:42–48. [PubMed: 7710647]

Gorno-Tempini ML, Dronkers NF, Rankin KP, Ogar JM, Phengrasamy L, Rosen HJ, Johnson JK, Weiner MW, Miller BL. Cognition and anatomy in three variants of primary progressive aphasia. Annals of Neurology. 2004; 55:335–346. [PubMed: 14991811]

Grimmer T, Diehl J, Drzezga A, F√∂rstl H, Kurz A. Region-Specific Decline of Cerebral Glucose Metabolism in Patients with Frontotemporal Dementia: A Prospective 18 F-FDG-PET Study. Dementia and Geriatric Cognitive Disorders. 2004; 18:32–36. [PubMed: 15084791]

Grossman M, McMillan C, Moore P, Ding L, Glosser G, Work M, Gee J. What's in a name: voxel-based morphometric analyses of MRI and naming difficulty in Alzheimer's disease, frontotemporal dementia and corticobasal degeneration. Brain. 2004; 127:628–649. [PubMed: 14761903]

Hagler DJ Jr, Saygin AP, Sereno MI. Smoothing and cluster thresholding for cortical surface-based group analysis of fMRI data. NeuroImage. 2006; 33:1093–1103. [PubMed: 17011792]

Hayasaka S, Du AT, Duarte A, Kornak J, Jahng GH, Weiner MW, Schuff N. A non-parametric approach for co-analysis of multi-modal brain imaging data: application to Alzheimer's disease. NeuroImage. 2006; 30:768–779. [PubMed: 16412666]

Horn JF, Habert MO, Kas A, Malek Z, Maksud P, Lacomblez L, Giron A, Fertil B. Differential automatic diagnosis between Alzheimer's disease and frontotemporal dementia based on perfusion SPECT images. Artif Intell Med. 2009; 47:147–158. [PubMed: 19481429]

Hunter R, Merrick M, Ferrington C, Notghi A, McLuskie R, Christie J, Goodwin G. Cerebral vascular transit time in Alzheimer's disease and Korsakoff's psychosis and its relation to cognitive function. The British Journal of Psychiatry. 1989; 154:790–796. [PubMed: 2557110]

Ishii K, Sakamoto S, Sasaki M, Kitagaki H, Yamaji S, Hashimoto M, Imamura T, Shimomura T, Hirono N, Mori E. Cerebral Glucose Metabolism in Patients with Frontotemporal Dementia. J Nucl Med. 1998; 39:1875–1878. [PubMed: 9829574]

Jeong Y, Cho SS, Park JM, Kang SJ, Lee JS, Kang E, Na DL, Kim SE. 18F-FDG PET Findings in Frontotemporal Dementia: An SPM Analysis of 29 Patients. J Nucl Med. 2005; 46:233–239. [PubMed: 15695781]

Johnson KA, Albert MS. Perfusion abnormalities in prodromal AD. Neurobiol Aging. 2000; 21:289–292. [PubMed: 10867213]

Johnson NA, Jahng GH, Weiner MW, Miller BL, Chui HC, Jagust WJ, Gorno-Tempini ML, Schuff N. Pattern of cerebral hypoperfusion in Alzheimer disease and mild cognitive impairment measured with arterial spin-labeling MR imaging: initial experience. Radiology. 2005; 234:851–859. [PubMed: 15734937]

Kanetaka H, Matsuda H, Asada T, Ohnishi T, Yamashita F, Imabayashi E, Tanaka F, Nakano S, Takasaki M. Effects of partial volume correction on discrimination between very early Alzheimer's dementia and controls using brain perfusion SPECT. Eur J Nucl Med Mol Imaging. 2004; 31:975–980. [PubMed: 14991240]

Knopman DS, Kramer JH, Boeve BF, Caselli RJ, Graff-Radford NR, Mendez MF, Miller BL, Mercaldo N. Development of methodology for conducting clinical trials in frontotemporal lobar degeneration. Brain. 2008; 131:2957–2968. [PubMed: 18829698]

Kril JJ, Halliday GM. Clinicopathological Staging of Frontotemporal Dementia Severity: Correlation with Regional Atrophy. Dementia and Geriatric Cognitive Disorders. 2004; 17:311–315. [PubMed: 15178943]

Lee C, Lopez OL, Becker JT, Raji C, Dai W, Kuller LH, Gach HM. Imaging cerebral blood flow in the cognitively normal aging brain with arterial spin labeling: implications for imaging of neurodegenerative disease. J Neuroimaging. 2009; 19:344–352. [PubMed: 19292827]

Li Y-O, Adal T.l. inodot, Calhoun VD. Estimating the number of independent components for functional magnetic resonance imaging data. Human Brain Mapping. 2007; 28:1251–1266. [PubMed: 17274023]

Lorenzen, P.; Davis, B.; Joshi, S. Med Image Comput Comput Assist Interv Int Conf Med Image Comput Comput Assist Interv. 2005. Unbiased atlas formation via large deformations metric mapping; p. 411-418.

Mioshi E, Hsieh S, Savage S, Hornberger M, Hodges JR. Clinical staging and disease progression in frontotemporal dementia. Neurology. 2010; 74:1591–1597. [PubMed: 20479357]

Mummery CJ, Patterson K, Price CJ, Ashburner J, Frackowiak RSJ, Hodges JR. A voxel-based morphometry study of semantic dementia: Relationship between temporal lobe atrophy and semantic memory. Annals of Neurology. 2000; 47:36–45. [PubMed: 10632099]

Nagao M, Sugawara Y, Ikeda M, Fukuhara R, Hokoishi K, Murase K, Mochizuki T, Miki H, Kikuchi T. Heterogeneity of cerebral blood flow in frontotemporal lobar degeneration and Alzheimer's disease. Eur J Nucl Med Mol Imaging. 2004; 31:162–168. [PubMed: 15129697]

Neary D, Snowden JS, Gustafson L, Passant U, Stuss D, Black S, Freedman M, Kertesz A, Robert PH, Albert M, Boone K, Miller BL, Cummings J, Benson DF. Frontotemporal lobar degeneration: A consensus on clinical diagnostic criteria. Neurology. 1998; 51:1546–1554. [PubMed: 9855500]

Rabinovici GD, Seeley WW, Kim EJ, Gorno-Tempini ML, Rascovsky K, Pagliaro TA, Allison SC, Halabi C, Kramer JH, Johnson JK, Weiner MW, Forman MS, Trojanowski JQ, DeArmond SJ, Miller BL, Rosen HJ. Distinct MRI Atrophy Patterns in Autopsy-Proven Alzheimer's Disease and Frontotemporal Lobar Degeneration. American Journal of Alzheimer's Disease and Other Dementias. 2008; 22:474–488.

Rosen HJ, Allison SC, Schauer GF, Gorno-Tempini ML, Weiner MW, Miller BL. Neuroanatomical correlates of behavioural disorders in dementia. Brain. 2005; 128:2612–2625. [PubMed: 16195246]

Rosen HJ, Gorno-Tempini ML, Goldman WP, Perry RJ, Schuff N, Weiner M, Feiwell R, Kramer JH, Miller BL. Patterns of brain atrophy in frontotemporal dementia and semantic dementia. Neurology. 2002; 58:198–208. [PubMed: 11805245]

Schroeter ML, Stein T, Maslowski N, Neumann J. Neural correlates of Alzheimer's disease and mild cognitive impairment: a systematic and quantitative meta-analysis involving 1351 patients. NeuroImage. 2009; 47:1196–1206. [PubMed: 19463961]

Schuff N, Zhu X. Imaging of mild cognitive impairment and early dementia. Br J Radiol. 2007; 80:S109–114. [PubMed: 18445740]

Shimizu S, Zhang Y, Laxamana J, Miller B, Kramer J, Weiner M, Schuff N. Concordance and Discordance Between Brain Perfusion and Atrophy in Frontotemporal Dementia. Brain Imaging and Behavior. 2010; 4:46–54. [PubMed: 20503113]

Shinagawa S, Ikeda M, Fukuhara R, Tanabe H. Initial Symptoms in Frontotemporal Dementia and Semantic Dementia Compared with Alzheimer‚Äôs Disease. Dementia and Geriatric Cognitive Disorders. 2006; 21:74–80. [PubMed: 16340203]

Steyn HS, Ellis SM. Estimating an Effect Size in One-Way Multivariate Analysis of Variance (MANOVA). Multivariate Behavioral Research. 2009; 44:106–129.

Sui J, Adali T.l. Pearlson GD, Clark VP, Calhoun VD. A method for accurate group difference detection by constraining the mixing coefficients in an ICA framework. Human Brain Mapping. 2009; 30:2953–2970. [PubMed: 19172631]

Tosun D, Mojabi P, Weiner MW, Schuff N. Joint analysis of structural and perfusion MRI for cognitive assessment and classification of Alzheimer's disease and normal aging. NeuroImage. 2010; 52:186–197. [PubMed: 20406691]

Van Leemput K, Maes F, Vandermeulen D, Suetens P. Automated model-based bias field correction of MR images of the brain. Medical Imaging, IEEE Transactions on 18. 1999a:885–896.

Van Leemput K, Maes F, Vandermeulen D, Suetens P. Automated model-based tissue classification of MR images of the brain. Medical Imaging, IEEE Transactions on 18. 1999b:897–908.

Varma AR, Adams W, Lloyd JJ, Carson KJ, Snowden JS, Testa HJ, Jackson A, Neary D. Diagnostic patterns of regional atrophy on MRI and regional cerebral blood flow change on SPECT in young onset patients with Alzheimer's disease, frontotemporal dementia and vascular dementia. Acta Neurologica Scandinavica. 2002; 105:261–269. [PubMed: 11939938]

Varrone A, Pappata S, Caraco C, Soricelli A, Milan G, Quarantelli M, Alfano B, Postiglione A, Salvatore M. Voxel-based comparison of rCBF SPET images in frontotemporal dementia and Alzheimer's disease highlights the involvement of different cortical networks. Eur J Nucl Med Mol Imaging. 2002; 29:1447–1454. [PubMed: 12397463]

Wen-Chau W, Edlow BL, Elliot MA, Jiongjiong W, Detre JA. Physiological Modulations in Arterial Spin Labeling Perfusion Magnetic Resonance Imaging. Medical Imaging, IEEE Transactions on 28. 2009:703–709.

Whitwell JL, Josephs KA, Rossor MN, Stevens JM, Revesz T, Holton JL, Al-Sarraj S, Godbolt AK, Fox NC, Warren JD. Magnetic Resonance Imaging Signatures of Tissue Pathology in Frontotemporal Dementia. Arch Neurol. 2005; 62:1402–1408. [PubMed: 16157747]

Worsley KJ, Taylor JE, Tomaiuolo F, Lerch J. Unified univariate and multivariate random field theory. NeuroImage. 2004; 23:S189–S195. [PubMed: 15501088]

Highlights

1. Enhanced description of pathophysiological changes in bvFTD with multimodality MRI
2. Greater effect size by joint ICA relative to unimodality image analysis
3. Multimodality imaging signatures to better assist diagnosis of dementia

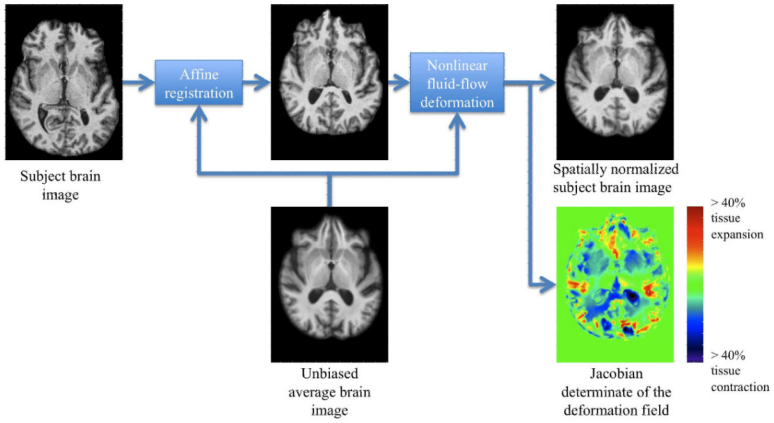

Figure 1.
Block diagram outlining the processing steps involved in deformation-based morphometry.

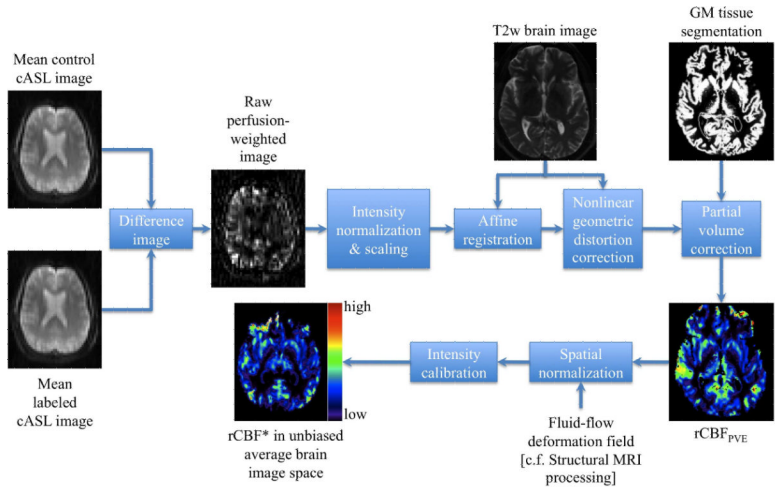

Figure 2.

A block diagram outlining the integrated multimodality image processing for perfusion-weighted MRI to estimate partial volume corrected regional cerebral blood flow.

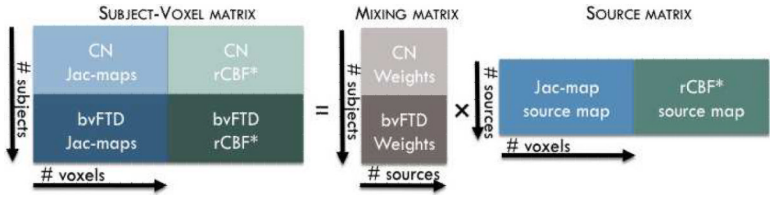

Figure 3.
The setup for multimodality joint independent component analysis.

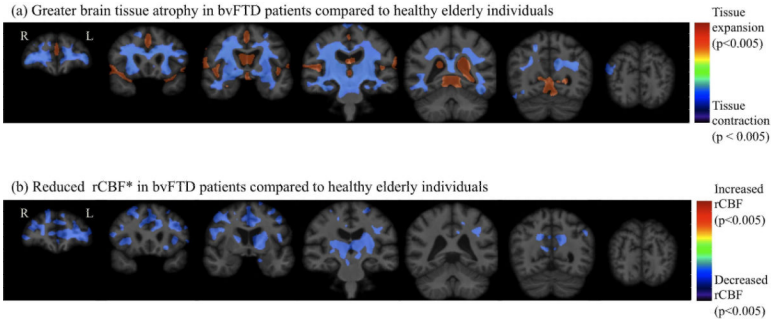

Figure 4.

Significance maps of systematic brain abnormalities in patients with behavioral variant frontotemporal dementia compared to controls using *unimodality* group difference analysis.

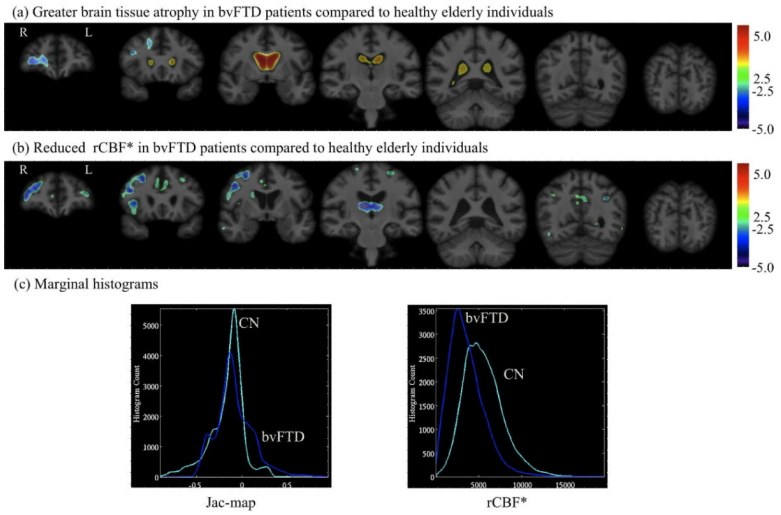

Figure 5.

The spatial extend of *1st joint component's* (a) Jac-map measure of brain tissue loss and (b) rCBF* features at z=2.5 threshold overlaid onto the unbiased average structural brain image. (c) Marginal histograms for the Jac-map and rCBF* measures.

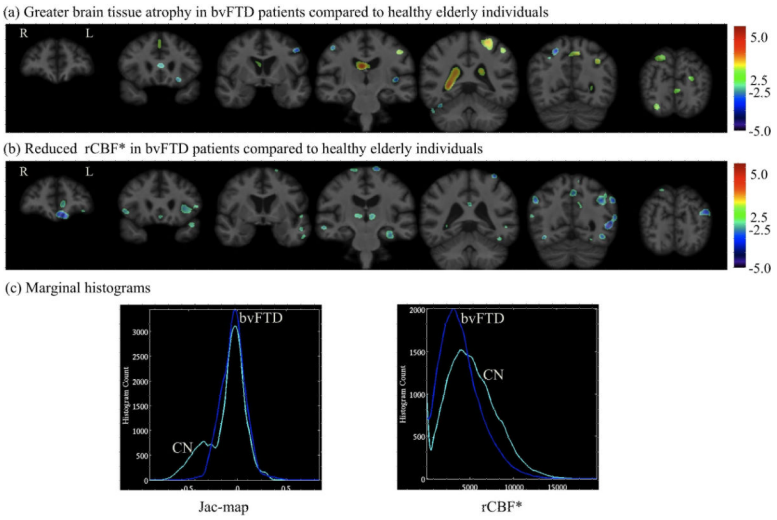

Figure 6.

The spatial extend of *2nd joint component's* (a) Jac-map measure of brain tissue loss and (b) rCBF* features at z=2.5 threshold overlaid onto the unbiased average structural brain image. (c) Marginal histograms for the Jac-map and rCBF* measures.

Table 1

Demographic and clinical summary of the study groups

	Control	Behavioral variant frontotemporal dementia
Number	12	12
Age	60.9 ± 7.6	60.3± 7.6
Sex (F:M)	3 : 9	3 : 9
Education (yr)	17.1 ± 2.6	15.5 ± 3.3
Durations of Symptom (yr)	—	6.1 ± 4.7
MMSE	29.6 ± 0.5	25.8 ± 3.8*
CDR	0	1.04 ± 0.3*

* Significantly differ from control group ($p<0.05$ by ANOVA test).

Table 2

List of brain areas where the structural and cerebral blood flow changes occur

Structural findings in behavioral variant frontotemporal dementia patients compared to controls	Cerebral blood flow findings in behavioral variant frontotemporal dementia patients compared to controls
Unimodal voxel-by-voxel Group Differences	
Greater ventricular enlargement	Reduced regional cerebral blood flow in bilateral
Greater brain tissue loss in bilateral	
superior frontal	superior frontal
middle frontal	middle frontal
inferior frontal	inferior frontal
lateral fronto-orbital	lateral fronto-orbital
middle fronto-orbital	middle fronto-orbital
cingulate	pre-cuneus
precuneus	cingulate
fornix	fornix
superior temporal	insula
middle temporal	parahippocampal
inferior temporal	supramarginal
parahippocampal	precentral
lingual	postcentral
fusiform	superior temporal
entorhinal	middle temporal
supramarginal	thalamic nuclei
superior parietal	putamen
inferior parietal	caudate
insula	hippocampus
precentral	
postcentral	
middle occipital	
inferior occipital	
cuneus	
cerebellum	
thalamus nuclei	
putamen	
caudate nucleus	
amygdala	
hippocampus	
1st Multimodality Joint Independent Components Analysis	
Greater ventricular enlargement	Reduced regional cerebral blood flow
Greater brain tissue loss in	bilateral middle frontal
right superior frontal	bilateral anterior cingulate
right middle frontal	bilateral caudate nucleus

Structural findings in behavioral variant frontotemporal dementia patients compared to controls	**Cerebral blood flow findings in behavioral variant frontotemporal dementia patients compared to controls**
right inferior frontal	bilateral thalamic nuclei
right lateral fronto-orbital	right superior frontal
right middle fronto-orbital	right inferior frontal
right gyrus rectus	right middle fronto-orbital
right anterior cingulate gyrus	right lateral fronto-orbital
right fornix	right insular
right insular	bilateral thalamus nuclei
right subcallosal area	
bilateral caudate nucleus	
2nd Multimodality Joint Independent Components Analysis	
Greater ventricular enlargement	Reduced regional cerebral blood flow
Greater brain tissue loss in	left supramarginal
left precentral	left superior temporal
left postcentral	left middle temporal
left superior parietal	bilateral superior parietal
left posterior cingulate	bilateral superior frontal
left fornix	bilateral gyrus rectus
left pre-cuneus	bilateral thalamus nuclei marginally in
right fusiform	bilateral posterior cingulate
right lingual	left inferior frontal
bilateral superior frontal	left lateral fronto-orbital
bilateral hippocampus	bilateral insular
	bilateral middle fronto-orbital
	bilateral postcentral
	left fusiform
	left parahippocampus
	bilateral middle occipital
	bilateral superior occipital
	bilateral inferior parietal
	bilateral hippocampus

Table 3

Effect sizes from 1st and 2nd components of a jICA compared to the effect size from conventional unimodal tests. Group differences are based on a generalized Fisher's correlation ratio.

	Wilks' lambda	Chi^2	η^2_Λ
1st joint component	0.531 ± 0.107	7.994 ± 2.369	0.468 ± 0.107
2nd joint component	0.613 ± 0.128	6.515 ± 2.891	0.387 ± 0.128
Unimodal tests	0.767 ± 0.114	3.458 ± 1.948	0.233 ± 0.114